An integrated workflow for MICP integration, pore typing and saturation height modeling – Poster # 62

Philippe Rabiller (Rabiller Geo-Consulting)

This paper was prepared for a presentation at the International Symposium of the Society of Core Analysts held in Vienna, Austria, 27 August – 1 September 2017.

ABSTRACT

Improving the integration and interpretation of MICP with other petrophysical and geological data is crucial to increase the efficiency and the reliability of: pore typing, saturation-height modeling and evaluation of the cap-rocks efficiency. In this view, the workflow and the modular suite of processes, illustrated here, were specifically designed for a seamless integration of Capillary Pressure data with logs and core data. They were successfully field tested (> 4000 MICP) in varied geological settings. They drastically minimize the user bias because they do not impose any predefined interpretative model of MICP curves such as "Thomeer's hyperbola" or "Gaussian fitting functions" while allowing the integration of the results of such models.

A regular re-sampling of the saturation data as a function of the pressure is the first step of the processes. It is followed by an automated (and editable) conformance correction and detection of "features of interest" in the drainage pore throat size distribution (PSD) curves, e.g.: picking of the Katz & Thompson Threshold and Entry Pressure. The regular resampling allows displaying the data in the classic layouts and X-plots views, with other logs. It makes possible all the subsequent processes, particularly the varied permeability models and the use of clustering, data prediction and histogram up-scaling techniques. By means of the latter techniques, a PSD log, regularly sampled with depth, can be created over the entire logged intervals of cored and un-cored wells and the predicted PSD can be up-scaled from plug to log or bed scale. In the final steps, the saturation, at any depth increment above Free Water Level, is computed by simply reversing the method used to derive PSD from MICP saturation curves and using the Pc equating the buoyancy forces at this depth increment; other methods can be used as well.

INTRODUCTION

The workflow presented here was developed for a seamless integration of MICP data with logs and core data with the aim to simplify the tasks of geoscientists, by letting them visualize, along with all logs and core data, their MICP data and use them for saturation height modeling, evaluation of rock sealing efficiency and, in first place, for pore typing and facies characterization. Indeed, unless MICP data are visualized and integrated with all available information, the characterization of rocks in terms of the relationship between porosity, permeability and texture is incomplete and the subsequent inferences based on rock facies and properties, are lacking the accuracy so much needed. Thus, the workflow is designed so as to:

- Maximize the possibilities to save, process, visualize (on depth display and X-plot) and edit the MICP data together with logs and core data into a single "host" software.

- Integrate the varied methods published on MICP processing and benefit from all.
- Benefit of cluster analysis and data prediction techniques.
- Minimize the user bias and the need for expertise.

So far, this workflow has been used well over 4000 MICP samples, of varied vintage, in varied formations from varied basins. Given the format of this paper, only the most important and innovative functionalities applied to drainage curves are illustrated.

DESCRIPTION OF THE WORKFLOW

Figure 1 summarizes the workflow, described below.

Stage 1: Creating the Saturation Array Log.

Stage 1 is carried in single well mode. Labs format the MICP data as spreadsheets, where mercury saturation is listed by irregular steps of injection pressure. Those data may be of varied vintage and varied range of pressure with varied and irregular pressure increments. Their integration requires that, in a first step, they are collated, well by well, into spreadsheets, where the lines are ordered by increasing depth and the pressure and saturation values are listed in columns indexed in the order of the pressure increment. The first column must list the depth of each sample.

Presenting the MICP data into a standard format suitable for display (Figure 2) and process, in single or multi-well modes, is achieved by "binning" the Hg saturation values into an array log whose bins are regular intervals of the logarithm of Pc. By default, the array log is 240 bins and covers the 100,000 psi to 0.1 psi pressure range, i.e.: pore throat (PT) radius from 0.001092µm to 1092 µm. Bins with "missing" values are filled by linear interpolation and the saturation curve is smoothed by an adjustable sliding window. The possibility is offered to evaluate the effect of binning and smoothing. With the default options, this effect is negligible and independent of the Pore Throat Radius (PTR).

Stage 2: Conformance Correction and Picking of Entry Pressure

The surface effects are corrected in 2 steps. In a first step, the pressure at conformance is picked by an algorithmic analysis of the shape of the saturation and PSD curves, considered jointly. The conformance correction is kept sufficiently mild so as to optimize the algorithmic picking of the entry pressure, performed in the second step, along the criteria illustrated by Katz & Thompson [1]. The output of each step is comprised of 2 QC indexes flagging those samples which do not fit the predefined quality criteria of the picking, in which case the user may discard the sample(s) or graphically edit their correction, before applying the corrections to the whole set of data. Permeability is very sensitive to the largest pore throats of the PSD; thus, if conformance and entry pressure corrections are wanting, a poor match between the measured and modeled permeability should invite to re-examine the corrections applied and iterate this stage.

Stage 3: Analysis of the Shape of the PSD Curve.

The 3rd stage, is devoted to the detection of the "features of interest" in the shape of the PSD. The flowchart in Figure 1 shows that this stage is performed twice:

- On the original PSD and in single-well mode, during the "plug scale" stage,

- On the Predicted and Up-scaled PSD, in multi-well mode, before performing saturation height modeling.

The primary "features of interest" of the PSD curves, shown in track 4 of figure 2, are their local minima, maxima and inflexion points. They are picked by searching for the "zero crossing", of the 1st, 2nd and 3rd order piecewise derivatives. The number and position of such features help quantifying the complexity of the porous network.

There are 2 very important features, namely:

- the Katz & Thompson Threshold which is "*the inflection point of the [saturation] curve [..]at which the mercury first forms a cluster spanning the sample [as established] by continuously monitoring the electrical resistance across the sample and determining the pressure where electrical continuity is made*".
- the apex of the Thomeer's hyperbola which, as summarized by Pittman [2] is "*the position on the mercury injection curve that represents a continuous, well-interconnected pore system through the rock. […Swanson] noted that at this point, "the mercury saturation expressed as percent of bulk volume is indicative of* ***that portion of the space effectively contributing to fluid flow***."

The second feature is picked by an algorithmic implementation of the trial solutions proposed by Katz & Thompson [1], Pittman [2], Walls & Amaefule [3] and Nokken & Hooton [4]. The track 9 of figure 2 illustrates the fact that the result of the trial solution for "maximal electrical conductance" corresponds exactly with the results of the picking of the other trial solutions. Not only this is a good indication that the tabulation technique is not distorting the data, but because the PSD and the "electrical maximal conductance" trial solution share the same array format, the latter trial solution simplifies the picking of the same feature on the Up-scaled PSD. This second feature is used to partition the PSD in 2 parts: the part which doesn't contribute to the permeability and the part which actually does contribute to permeability and hence to the production through permeability mechanism. This partition is a key element of a new version of the Purcell model.

Stage 4: Purcell-PSKT Permeability Modeling.

The 4th stage is devoted to the characterization, at plug scale, of the porosity/permeability relationships. To that purpose, the Purcell equation is implemented along 3 modalities:

- the first modality, is the classic form of the Purcell equation [5].
- In the second modality, the Purcell equation is applied to each term of the suite of the PTR subsets formed by incrementing the first subset by 1 element of the PSD: $PTR_{[a]}$, $PTR_{[a \rightarrow (a+1)]}$, $PTR_{[a \rightarrow (a+2)]}$, $PTR_{[a \rightarrow (a+3)]}$, ….., $PTR_{[a \rightarrow (n)]}$ Where "a" is the first (smallest radius) element of the PSD array log, with a significant value, and "n" is the last one (corresponding to "entry pressure").
- The third modality, termed "Purcell-PSKT" model, is similar to the second but the first term of the suite of PTR subsets is the PSD element which corresponds to the apex of the Thomeer's hyperbola. Thus, by taking into account only the PTR subset which actually contribute to the permeability the Purcell-PSKT model honors the results of Pittmann [2], Swanson [6], Katz & Thompson [1], Walls & Amaefule [3].

Not only the Purcell-PSKT model predicts the permeability better than the Purcell model proper [7], but most importantly, it allows generalizing to any complex porous network, the use of the FZI method, introduced by Amaefule and his co-workers [8], which postulates that the porosity is "effective" in terms of permeability. In this conceptual framework, the validity of the derivation of PHI_Z by the Purcell-PSKT model is verified by using the Darcy and Poiseuille equations in the way proposed by Amaefule for the FZI theory: if the Darcy and Poiseuille equations are honored then a straight line must appears when X-plotting FZI (X axis) versus the ratio r_{mh}/PHI_Z, where "r_{mh}" is the Mean Hydraulic Radius. Consequently, PHI_Z should be used, instead of total porosity PHI_T, in the equations proposed by Leverett [9] or Amaefule & al.[8] to predict S_w from P_c.

The 2nd part of the 4th stage, is devoted to porosity typing: the PSD and the distribution of the contribution of each PTR to the permeability are "binned" into array logs whose bins are regular increments of increasing porosity and are grouped into 5 editable classes defined by their PTR range of radius (µm), namely: Nano: ($r < 0.1$), Micro: ($0.1 < r < 0.5$), Meso: ($0.5 < r < 2$), Macro: ($2 < r < 10$) and Mega: ($r > 10$). Two such array logs are created: one for PHI_T, the other for PHI_Z, as shown in tracks 8 & 9 of Figure 3; they ease the comparisons of MICP data with descriptions of core, fine scale core data and thin sections, other logs and borehole imagery logs which mostly respond to porosity.

Stage 5: Application of Up-Scaling, Clustering and Prediction Techniques

In the view of defining RRT, a 3 step approach is proposed, whose application to the evaluation of the sealing efficiency of rocks was previously illustrated [10; 11]. It is based on the use of:

- "Multi Resolution Graph Based Clustering" (MRGC) and "Coarse to Fine Self Organized Map Ordering" (CFSOM) [12; 13] for the grouping of MICP data into Reservoir Rock Types (RRT). The result of such clustering is illustrated by Figure 4.
- "k-Nearest Neighbor" (k-NN) modeling for prediction, of the PSD, RRT, permeability, PHI_Z and FZI. This method allows carrying simultaneously, the predictions of all those predict and testing both the validity of its results and the applicability of the prediction model [14]. By predicting the actual PSD, with the appropriate predictors, a PSD log regularly sampled with depth, is generated over the whole logged intervals, even in un-cored wells. The use of k-NN modeling in this field of work is reported, for example, by Theologou and his co-workers [15].
- Histogram Up-scaling method, [16] which is used in the following way to account for the heterogeneities between plug scale and log scale. Let's consider a depth increment "A" in the logged interval of a well; "A" being characterized by a set of log readings (its coordinates in the n-dimensional log space) and by a real or a predicted PSD. By means of the k-NN method, the "k" depth increments most similar to "A", i.e.: its "k" nearest neighbors in the log space, can be retrieved together with their PSD (real or predicted) and presented by order of increasing distance from "A" in the log space, i.e.: by decreasing similarity with "A". By optimizing a threshold on this distance it is possible to select the PSD of only those depth increments whose log readings are considered sufficiently similar to "A". The selected PSD may be similar and hence it

may be inferred that they belong to some facies homogeneous at log scale; if they differ significantly then the facies they belong to is heterogeneous; how much they differ is quantifiable. In both cases, a summation and volume weighted averaging allows up-scaling the selected PSD for they are scalar variables.

Eventually the stages 3 and 4 described above should be iterated on the up-scaled predicted PSD which is used in stage 6 as input for Saturation/Height Modeling.

Stage 6: Saturation Height modeling.

The figure 5 illustrates how Saturation Height Modeling is performed by reversing the method used to derive PSD and applying it onto the up-scaled PSD, regularly sampled with depth. The input required are:

- the density (constant or variable with field conditions), of hydrocarbon(s) and brine
- the Hc/brine IFT and contact angle (constant or variable with field conditions).

In a first step, for each depth increment of the entire logged interval, the array log of "Saturation vs Pc" is computed by piecewise integration of the up-scaled PSD. Then, ΔP_c developed by buoyancy forces at each depth increment is computed for any given position, or for a suite of regularly incremented positions, of the FWL. Finally, ΔP_c is used to scan and test the "Saturation vs Pc" array log so as to: retrieve the saturation, compute a dynamic permeability cut off, and estimate the volume of Hc which can be mobilized by permeability mechanism [7]. The superimposition of a Pc_{field} scale onto the PSD, permeability and saturation arrays logs in the graphic display of the output relies on the Pc/radius equivalence, for any couple of fluids whose IFT and contact angle are specified for lab and field conditions.

CONCLUSIONS.

The figures illustrating the workflow evidence the feasibility to load and format the MICP data, process them and display all the results in the conventional Depth and X-plot views of the petrophysical software commercially available. A seamless integration of MICP with other logs and core data and the use of clustering and prediction techniques are thus made possible.

The implementation of the trial solutions proposed by Katz & Thompson, Pittmann, Walls & Amaefule provides an accurate estimation of the porosity (PHI_Z) effectively contributing to the permeability, either from actual PSD or from the up-scaled PSD.

The new "Purcell-PSKT" model, specifically designed to combine the results of Katz & Thompson, Pittman, Walls & Amaefule with the Purcell equation, provides a better prediction of permeability than the Purcell model proper; thus, it gives a greater confidence in the picking of the "entry pressure". The Purcell-PSKT model allows the generalization of the FZI method to a complex porous network and the validity of its derivation of PHI_Z is corroborated by the same techniques proposed for the FZI method. By using PHI_Z instead of PHI_T, the Leverett and FZI theories should prove more effective to predict S_w as a function of Pc.

Saturation height modeling is greatly simplified by simply reversing the method used to derive PSD from the MICP saturation curves.

REFERENCES

1. Katz, A.J., A.H.,Thompson : "Prediction of Rock Electrical Conductivity from Mercury Injection Measurements"; Journal of Geophysical Research, Jan. 1987, Vol. 92, No.B1, 599-607.
2. Pittman, E.D. : "Relationship of Porosity and Permeability to Various Parameters Derived from Mercury Injection Capillary Pressure Curves for Sandstone," AAPG Bull., 1992, vol. 76, No. 2; 191-198.
3. Walls, J.D. & J.O., Amaefule : "Capillary Pressure and Permeability Relationships in Tight Gas Sands," ; 1985; paper SPE 13879.
4. Nokken M. R. & R. D. Hooton: "Using Pore Parameters to Estimate Permeability or Conductivity of Concrete"; Materials and Structures; 2006; DOI 10.1617/s11527-006-9212-y.
5. Purcell, W.R.: "Capillary Pressures-Their Measurement Using Mercury and the Calculation of Permeability"; 1949, Trans. AIME, 186, 39-48.
6. Swanson, B. F.; "A simple correlation between permeabilities and mercury capillary pressures"; 1981; Journal of Petroleum Technology, Dec., p. 2488-2504.
7. Rabiller, Ph.; "Combining porosimetry and Purcell permeability modeling to calibrate FZI and define a dynamic permeability cut off. Poster#26"; 2017; International Symposium of the Society of Core Analysts.
8. Amaefule J. O.; M. Altunbay M., D. Tiab; D. G. Kersey; D. K. Keelan, "Enhanced Reservoir Description: Using Core and Log Data to Identify Hydraulic (Flow) Units and Predict Permeability in Uncored Intervals/Wells"; 1993; paper SPE 26436.
9. Leverett M. C.; "Capillary Behavior in Porous Solids"; 1941; Transactions Of The American Institute Of Mining And Metallurgical Engineers; Volume 142; 152-168.
10. David Z. Tang, Ph. Rabiller, A. Bakhiet, G. Gregory, P. Lawrence, A. Samsudin, W. Tan; "Well-log Electrofacies Prediction of Middle and Upper Jurassic Carbonates, Saudi Arabia: A Case Study for Exploration Applications"; 2012; Geoarabia.
11. Rabiller, Ph.; "Integration of MICP Data with Logs, as a Means to Improve Reservoir and Seal Characterization"; 2017; Search and Discovery Article #42013.
12. YE, S-J., Ph. Rabiller; "A New Tool for Electro-Facies Analysis: Multi-Resolution Graph-Based Clustering"; 2000; SPWLA 41st annual symposium; paper PP; 1-14
13. YE, S.J. & Ph. Rabiller; "Automated facies Ordering"; 2005; Petrophysics; Vol. 46, n° 6; 409-423
14. Rabiller, Ph. ; P. Boles; N.H. Dewhirst; : "Facimage™ Modeling as a Substitute for Gas Content from Core Desorption and for Real Time Facies Analysis."; 2013; URTeC symposium (Denver); ID: 1580723
15. Theologou, P.; M. Skalisnski; R.K., Mallan; "An MICP based Pore typing workflow-Core scale to log scale" , paper L ; 2015; SPWLA, 56th Annual Symposium.
16. Rabiller, Ph.; J.P., Leduc; S.J., YE : "The iterative use of clustering and modeling to improve permeability prediction."; 2001; SPWLA 42nd annual symposium; paper E.

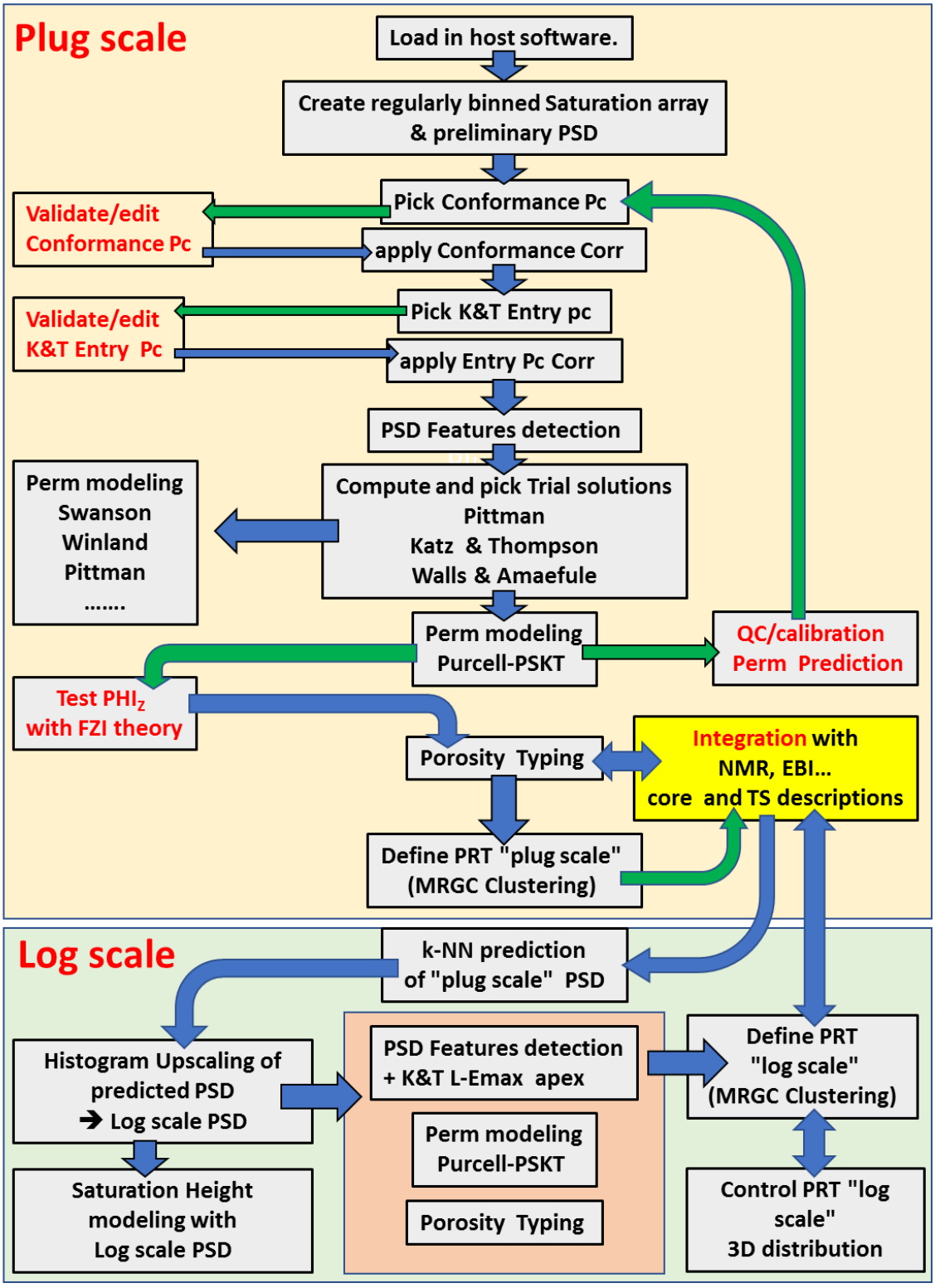

Figure 1 : Diagram of the workflow.

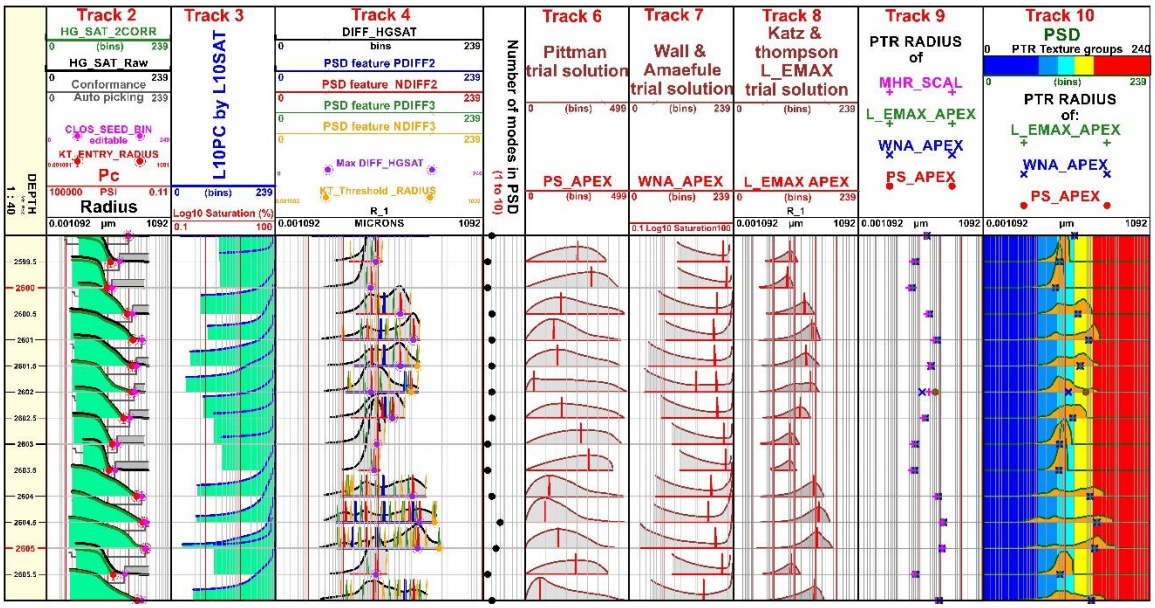

Figure 2 : The 2nd and 3rd tracks show the saturation displayed into a standard format suitable for any process. Conformance Correction and Picking of Entry Pressure are shown on 2nd track. The detection of the "features of interest" in the structure of the MICP data and the result of trial solutions are shown, respectively, in tracks 4, 6, 7, 8, 9.

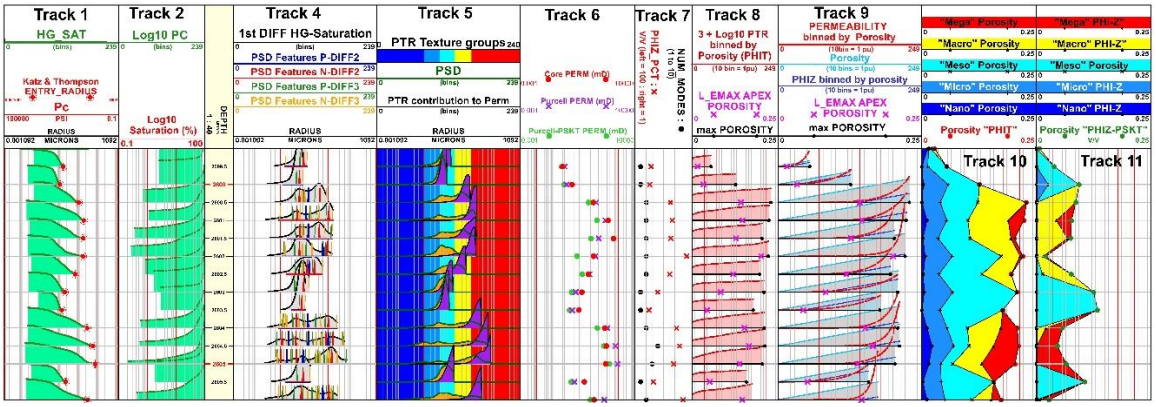

Figure 3: Track 5 shows the "contribution of PTR to permeability" superimposed to PSD, thus illustrating the fact that only largest PTR classes contribute to permeability. Core permeability and the results of permeability modeling are shown on track 6. The complexity of the porous network is illustrated by the PSD features (track 4), the number of modes and the ratio PHI_Z/PHI_T (track 7). On tracks 9 to 11, the PSD and contribution of PTR to permeability are "binned" by porosity and thus the contribution of each PTR groups to porosity (either PHI_T : track 10 or PHI_Z : track 11) is graphically illustrated for easier comparisons with descriptions of thin sections.

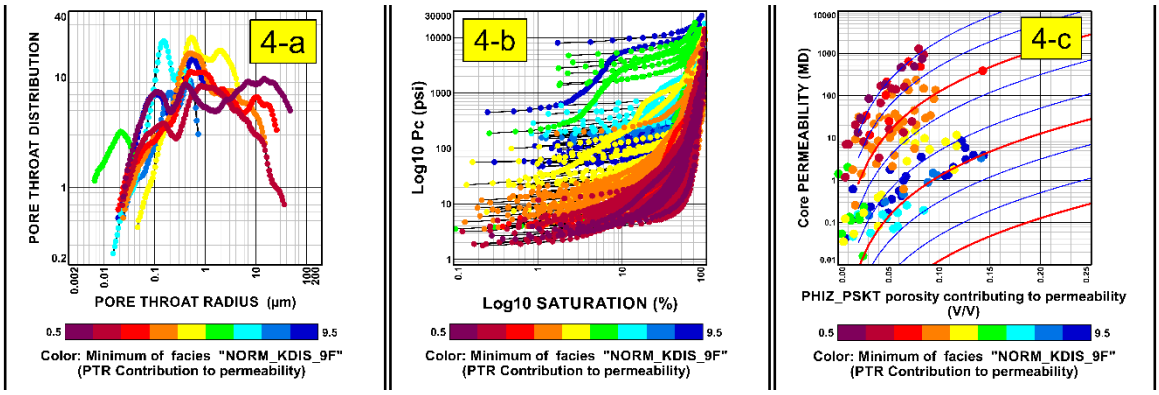

Figures 4a to c illustrate the application of MRGC clustering to MICP data and more specifically to "PTR contribution to permeability" which provides the most interesting classification in terms of pressure (Height) vs Saturation (4b) because it is PHI_Z, which controls the flow. X-plot 4a displays only the "kernel" of each facies. Clustering PSD provides insights on porous network texture, however PSD "facies" are less significant in terms of dynamic flow properties for flow is not controlled by PHI_T. The X-axis of the FZI plot (4c) is PHI_Z, note the good fit between facies and FZI curves.

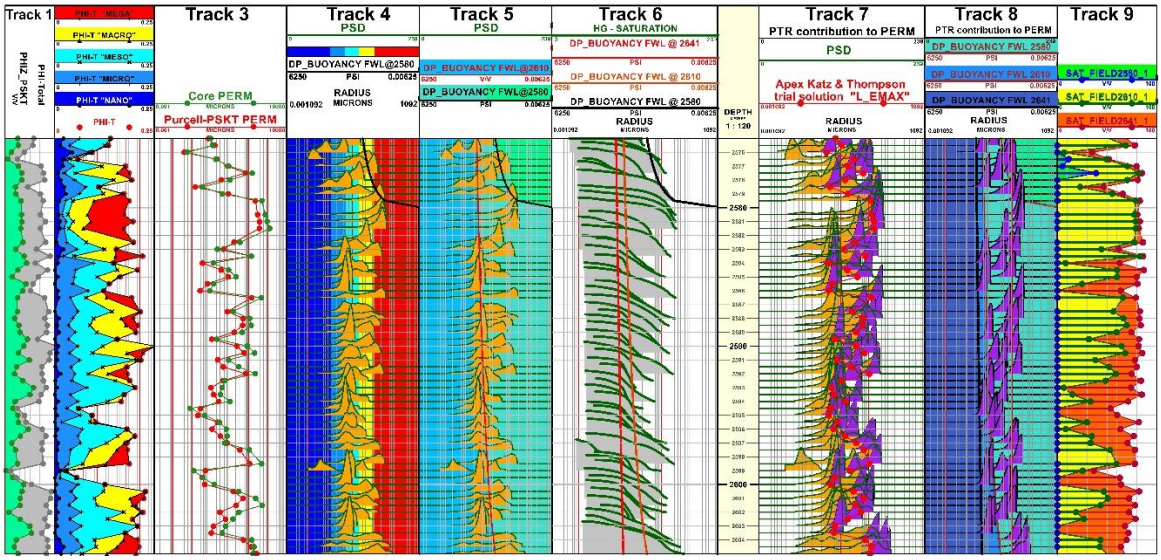

Figure 5: Saturation Height modeling. The rightmost track displays the saturation for 3 positions of the FWL. The saturation is obtained by equating the buoyancy force and the capillary pressure. Because saturation is sampled as a function of Pc, retrieving saturation for any position of FWL is made simple and accurate. The tracks 8 & 9 illustrate the fact that the most important reservoir characteristic is the distribution of the pore volume accessible by those pore throats which actually control the permeability. The tracks 4 & 5 & 8 illustrate the fact that a "static" description of pore network "texture" (track 4) is insufficient to explain fluid storage and flow, hence the importance of partitioning them by the PTR corresponding to Δp buoyancy (track 5).